Two motor neuron synergies, invariant across ankle joint angles, activate the triceps surae during plantarflexion

Jackson Levine[1, 2, 3, *], Simon Avrillon[1, 2, 4, *], Dario Farina[4], François Hug[5, 6], José L. Pons[1, 2, 3]

[1] Legs + Walking Lab, Shirley Ryan AbilityLab, Chicago 60611, IL, USA
[2] Department of Physical Medicine and Rehabilitation, Feinberg School of Medicine, Northwestern University, Chicago 60611, IL, USA.
[3] Department of Biomedical Engineering, McCormick School of Engineering, Northwestern University, Chicago 60611, IL, USA.
[4] Department of Bioengineering, Faculty of Engineering, Imperial College London, London W12 7TA, UK
[5] Université Côte d'Azur, LAMHESS, Nice 06200, France
[6] The University of Queensland, School of Biomedical Sciences, St Lucia QLD 4072, QLD, Australia

* These authors equally contributed to this work.

Short title: Invariance of common inputs to motor neurons

Correspondence:
Simon Avrillon
Imperial College London, London, UK
e-mail: s.avrillon@imperial.ac.uk
José L. Pons
Legs + Walking Lab, floor 23
Shirley Ryan AbilityLab, Chicago, IL, USA
e-mail: jpons@sralab.org

Number of pages: 32; Number of figures: 5

Conflict of interests:
The authors declare no competing financial interests.

Acknowledgements
Dario Farina is supported by the European Research Council Synergy Grant NaturalBionicS (contract #810346), the EPSRC Transformative Healthcare, NISNEM Technology (EP/T020970), and the BBSRC, "Neural Commands for Fast Movements in the Primate Motor System" (NU-003743). François Hug is supported by a fellowship from the French government, through the UCAJEDI Investments in the Future and by the National Research Agency (ANR) with the reference number ANR-15-IDEX-01. Jose L. Pons is supported by the National Science Foundation/National Robotics Initiative under Grant 2024488.

Abstract

Recent studies have suggested that the central nervous system generates movements by controlling groups of motor neurons (synergies) that do not always align with muscle anatomy. In this study, we determined whether these synergies are robust across tasks with different mechanical constraints. We identified motor neuron synergies using principal component analysis (PCA) and cross-correlations between smoothed discharge rates of motor neurons. In Part 1, we used simulations to validate these methods. The results suggested that PCA can accurately identity the number of common inputs and classify motor neurons according to the synaptic weights of the common inputs they receive. Moreover, the results confirmed that cross-correlation can separate pairs of motor neurons that receive common inputs from those that do not receive common inputs. In Part 2, sixteen individuals performed plantarflexion at three ankle angles while recording high-density surface electromyography from the gastrocnemius lateralis (GL) and medialis (GM) and the soleus (SOL) muscles. We identified and tracked the same motor units across angles. PCA revealed two motor neuron synergies, primarily grouping motor neurons innervating GL-SOL and GM-SOL. These motor neuron synergies were relatively stable with 74.0% of motor neurons classified in the same synergy across angles. Cross-correlation demonstrated that only 13.9% of pairs of motor neurons maintained a non-significant level of correlation across angles, confirming the large presence of common inputs. Overall, these results highlighted the modularity of movement control at the motor neuron level, which may ensure a sensible reduction of computational resources for movement control.

Significance statement:

The central nervous system may generate movements by activating clusters of motor neurons with common inputs. In line with this hypothesis, we show here that two main sources of common inputs drive the motor neurons innervating the triceps surae muscles during ankle plantarflexions. For the first time, we report that the distribution of these common inputs is globally invariant despite changing the mechanical constraints of the tasks, i.e., the ankle angle. These results demonstrate the functional relevance of the modular organization of the central nervous system to control movements.

Introduction

The neural control of movement relies on the coordinated activity of numerous motor units. A large proportion of these motor units receive common synaptic inputs (Laine et al., 2015; Negro et al., 2016a), which arise from various sources, including descending commands and proprioceptive feedback (Christakos et al., 2006; Lemon, 2008; Heckman and Enoka, 2012; Laine et al., 2014; Glover and Baker, 2022). Simulation studies showed that the pool of motor neurons tends to linearly transmit these common synaptic inputs to the muscle while it attenuates independent inputs (Farina et al., 2014b). Thus, the time-varying modulation of muscle force during a sustained contraction mainly depends on the modulation of common synaptic inputs, as evidenced by the significant correlation between the low-pass filtered cumulative spike train of motor units and muscle force (De Luca and Erim, 2002; Negro et al., 2009; Thompson et al., 2018).

When considering the coordination of multiple muscles, common synaptic inputs may also be distributed across groups of motor units that share a similar function to generate a force in a desired direction (Tresch and Jarc, 2009; Bizzi and Cheung, 2013). This distribution determines a modular organization with low dimensionality. This concept of *synergies* (or motor modules) has been mainly demonstrated at the muscle level by combining the recording of multiple muscles with bipolar electromyography and factorization algorithms (Tresch et al., 1999; d'Avella et al., 2003; Ting et al., 2015; Yaron et al., 2020). The implicit assumption of this approach is that all motor neurons innervating a muscle (i.e., a motor neuron pool) receive the same common inputs. However, this assumption has been challenged by recent results. For example, it has been shown that motor neurons innervating a single muscle can be separated into several clusters based on their common fluctuations of discharge rate, even during tasks of a single degree of freedom (Madarshahian et al., 2020; Del Vecchio et al., 2022). These approaches at the motor neuron level revealed a new dimensionality of movement control, where (motor neuron) synergies can still span across muscles, but also cover subsets of motor neurons within each muscle or across portions of different muscles (Hug et al., 2022b).

To date, the identification of clusters in motor neuron activity, termed ‘motor neuron synergies’, has only been reported for single joint motor tasks with stable mechanical constraints (Madarshahian et al., 2020; Del Vecchio et al., 2022; Hug et al., 2022b). It remains unknown whether the distribution of common inputs to groups of motor neurons is robust across motor tasks,

100 as observed for muscle synergies (d'Avella et al., 2003). Addressing this question is fundamental
101 to prove that the observed clustering of motor neurons is an effective way of simplifying the neural
102 control of movement by modules that are invariant across a repertoire of tasks.

103 The technical challenge of identifying motor neuron clusters across tasks is that motor neuron
104 activities must be tracked across tasks using decompositions of high-density electromyographic
105 (HD-EMG) signals (Farina and Holobar, 2016; Negro et al., 2016b). However, HD-EMG
106 decomposition is currently only applicable during tonic contractions with slight changes in muscle
107 length since this procedure relies on the stability of muscle geometry to identify the unique
108 spatiotemporal properties of motor unit action potentials as detected by the grid of electrodes
109 (Martinez-Valdes et al., 2017; Vecchio and Farina, 2019; Oliveira and Negro, 2021). For these
110 reasons, we identified and tracked motor neurons innervating the triceps surae muscles (soleus
111 [SOL], gastrocnemius medialis [GM], and gastrocnemius lateralis [GL]) while muscle lengths were
112 altered by rotating the ankle. This change in muscle length resulted in altered muscle force
113 generating capacity. These muscles are of interest as there is evidence of uncoupling of their neural
114 drives during sustained contractions (Hug et al., 2021a; Rossato et al., 2022), despite all being
115 connected to the same distal tendon and being identified within the same motor module during
116 most natural behaviors. Similarly, it was shown that changes in neural drive due to the alteration
117 of force generating capacity during an ankle rotation may differ between GL and GM/SOL
118 (Lacourpaille et al., 2017). This suggests that the central nervous system could control more than
119 one synergy, even during a task with one degree of freedom (Lacourpaille et al., 2017; Rossato et
120 al., 2022).

121 In this study, we identified motor neuron synergies by estimating the distribution of common
122 synaptic inputs to the group of motor neurons innervating the triceps surae muscles using principal
123 component analysis and cross-correlation of their smoothed discharge rates (Fig. 1A). To validate
124 the analysis, we first simulated 100 motor neurons receiving two sources of common synaptic
125 input, and we assessed whether the proposed processing method could identify the low dimensional
126 control of motor neuron behavior. Following this validation, we recorded HD-EMG signals over
127 the triceps surae muscles across three ankle angles from 16 participants to evaluate the robustness
128 of motor neuron synergies across tasks. We hypothesized that 1) despite the single dimension
129 captured by classic electromyographic analysis, the dimensionality of control at the motor neuron
130 level would be greater than one, and 2) the structure of the identified motor neuron synergies would

remain invariant across joint angles. The validation of these hypotheses would provide evidence that the central nervous system controls movements by distributing common inputs to stable groups of motor neurons, ensuring a sensible reduction of computational resources needed to successfully complete this task.

Methods

Part 1: Simulations

We first aimed to test the sensitivity of our methods to capture the low dimensional control of motor neurons (Fig. 1B). As previous studies have shown differential changes in neural drive between GL and GM/SOL during constrained isometric plantarflexions (Lacourpaille et al., 2017; Hug et al., 2021a), we hypothesized that two main sources of common inputs may drive the triceps surae muscles during plantarflexion. Thus, we simulated 100 motor neurons receiving common and independent synaptic inputs using the model developed by Elias and Kohn (2013), with two compartments for the soma and the dendritic tree. This model is an updated version of a previously published motor neuron model (Cisi and Kohn, 2008) with the addition of a L-type Ca^{++} channel into the dendritic compartment to consider the non-linearity between motor neuron inputs and outputs due to persistent inward currents. Geometric and electronic parameters of the 100 motor neurons were linearly interpolated from the range of values reported in Table 1 of (Elias and Kohn, 2013) for a S-type motor unit.

The total synaptic input for each motor neuron was the linear summation of common and independent inputs simulated as white Gaussian noise. The common and independent inputs had equal variances, with a bandwidth of 0-2.5Hz for the common inputs, and a bandwidth of 0-50Hz for the independent inputs. The mean and the variance of the total synaptic input were tuned to generate physiologically realistic distributions of interspike intervals (Negro et al., 2016a). To simulate motor neuron synergies, we generated two uncorrelated sources of common synaptic inputs with a range of synaptic weights for the pool of motor neurons. Specifically, 20 motor neurons received 100% of common input (CI) #1, 20 motor neurons received 100% of CI#2, and 60 motor neurons received CI#1 and CI#2 with synaptic weights ranging from 99% CI#1/1% CI#2 to 1% CI#1/99% CI#2. The synaptic weights were shuffled across the 100 motor neurons and fixed for all the simulations.

We generated three simulations with different amplitudes of the two common inputs. In the first simulation, the amplitude of common inputs #1 and #2 were equal (CI#1 = CI#2). In the second (CI#1+ CI#2) and third simulations (CI#1++ CI#2), the amplitude of common input #1 was amplified to generate an averaged increase in discharge rate of 1 pps for all the motor neurons receiving this input (Fig. 1B). This idea was to mimic the divergent modulation of two separate

sources of common synaptic inputs and to match the discharge rates experimentally observed during the plantarflexions.

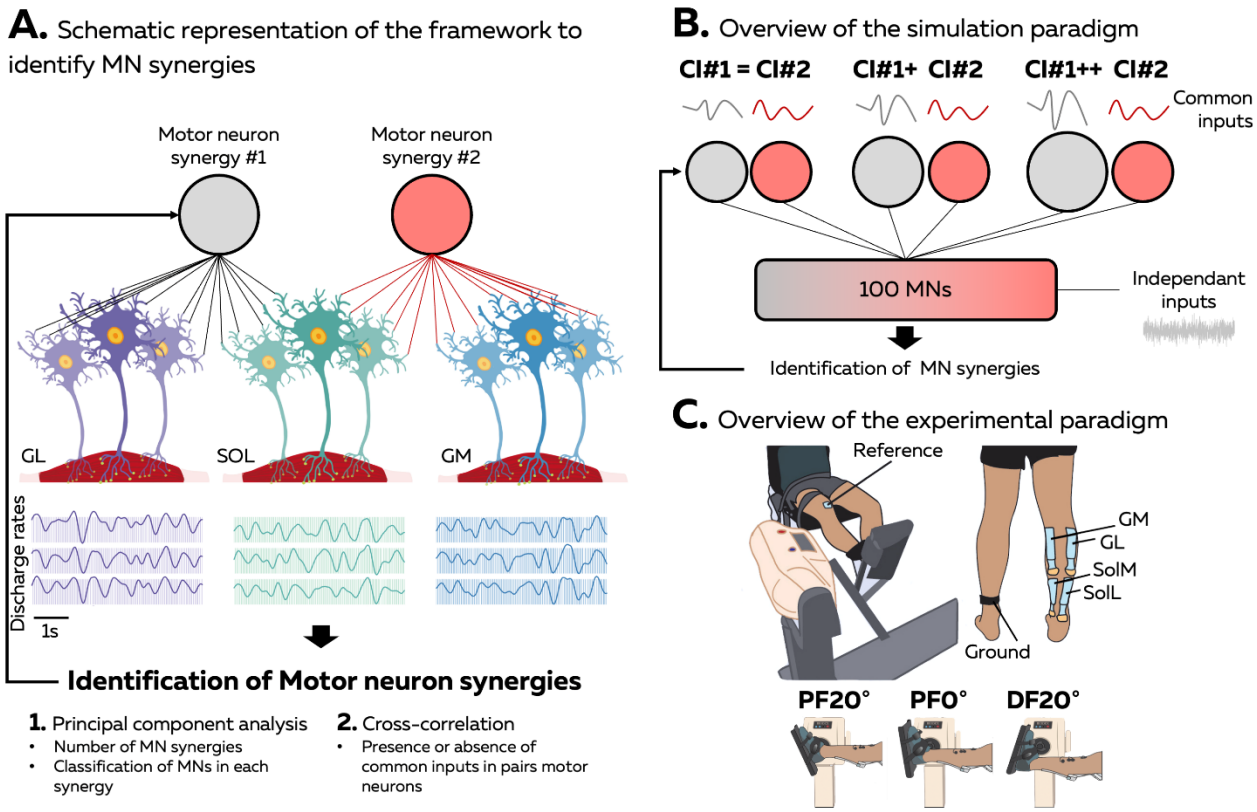

Figure 1: Overview of the study. We aimed to identify motor neuron synergies driving the triceps surae muscles during ankle plantarflexion. (A) We hypothesized that two motor neuron synergies would drive the gastrocnemius lateralis (GL), soleus (SOL), and gastrocnemius medialis (GM) muscles. To test this hypothesis, we needed to identify the distribution of common inputs to the pool of motor neurons. Thus, we applied principal component analyses (PCA) and cross-correlation on motor neuron smoothed discharge rates. (B) We first assessed the ability of these methods to identify the distribution of common inputs across motor neurons using 100 simulated motor neurons driven by two sources of common inputs with known synaptic weights. We changed the amplitude of these inputs to mimic the divergent variations in neural drive observed experimentally between GL and GM/SOL muscles. (C) Then, we identified and tracked motor units from high-density electromyographic signals recorded over the GL, GM, and SOL muscles across three ankle angles. As for the simulation, we determined whether the distribution of common inputs to the tracked motor units was robust across the three conditions using PCA and cross-correlation.

Part 2: Experiments

In the second part of the study, we identified and tracked the motor neuron synergies driving the triceps surae muscles during plantarflexions performed at three ankle joint angles (Fig. 1C).

184

185 ***Participants***

186 A sample of sixteen individuals, with an equal number of males (n = 8; age: 28 ± 4 years, height:
187 178 ± 6 cm, body mass: 77 ± 10 kg) and females (n = 8; age: 29 ± 11 years, height: 162 ± 8 cm,
188 body mass: 60 ± 9 kg), volunteered to participate in this experiment. They had no history of knee
189 nor ankle injury in the last six months before the experiments or lower leg pain that would impact
190 their ability to complete the voluntary contractions. The institutional review board (IRB) of
191 Northwestern University reviewed and approved the protocol of this study (STU00212191).
192 Participants provided their informed written consent before starting the experimental session.

193

194 ***Protocol***

195 Participants sat on a dynamometer (Biodex System 4 Pro, Biodex Medical, Shirley, NY) with their
196 hip flexed at 90º (0º being the neutral position) and their knee fully extended (Fig. 1C). The foot of
197 the dominant leg (i.e., right leg for all the participants) was fixed to a pedal that held the ankle at
198 specified angles (Fig. 1C). Two inextensible straps immobilized their torso, while additional straps
199 around the waist and the thigh of the dominant leg ensured that force generation solely relied on
200 the calf muscles.

201 All experimental tasks consisted of isometric ankle plantarflexion. The participants first performed
202 a standardized warm-up with their ankle positioned at neutral position (0º, i.e., the foot is
203 perpendicular to the shank). Participants were asked to push against the pedal with gradually
204 increasing effort, beginning at about 50% of their subjective maximum capabilities. After three
205 contractions, participants were asked to increase effort until they reached about 80-90% of their
206 subjective maximum capabilities.

207 After the warm-up, experimentation began. The experimental protocol was repeated for three
208 different conditions in a randomized order: the ankle plantarflexed at 20º (PF20°), at 0º (PF0°), and
209 dorsiflexed at 20º (DF20°) (Fig. 1C). For each condition, participants performed two maximal
210 isometric voluntary contractions (MVC) for 3-5 s, with 60 s of rest in between. The peak torque
211 was calculated using a moving average window of 250 ms, and the maximal value was used to set
212 the target of the submaximal isometric contractions at 20% of the MVC. After 60 s of rest,
213 participants performed three trapezoidal contractions, consisting of a 15 s linear ramp-up, 30 s
214 plateau at 20% of the MVC, and 15 s linear ramp-down. These three trapezoidal contractions were

separated by 10 s of rest. Target and torque output feedback were displayed on a monitor in front of the participants. The HD-EMG acquisition system (EMG-Quattrocento; 400-channel EMG amplifier, OT Bioelettronica, Italy) was used to digitize the torque signal at a sampling rate of 2048 Hz. Torque signals were low pass filtered (3rd order Butterworth filter, cutoff frequency: 20 Hz) and baseline corrected to remove the weight of the leg and the pedal. Torque accuracy was calculated as the root mean squared error (RMSE) of the signal over the plateau.

High-density surface EMG recording

High-density surface EMG (HD-EMG) signals were recorded from the gastrocnemius medialis (GM), gastrocnemius lateralis (GL), and the lateral and medial regions of the soleus (SOL) using two-dimensional adhesive grids of 64 electrodes (GR08MM1305, 13x5 gold-coated electrodes with one electrode absent on a corner; interelectrode distance: 8mm, OT Bioelettronica, Italy). The grids were aligned in the fascicle direction for the GM and GL. The grids over the soleus were positioned on each side of the Achilles tendon in the muscle shortening direction. Before placing the electrodes, the skin was shaved and cleaned with an abrasive pad and an alcohol wipe. A semi-disposable biadhesive foam layer was used to hold the grids of electrodes to the skin, and conductive paste filled the cavities of the adhesive layers to make skin-electrode contact. Reference electrodes (Ag/AgCl snap electrodes, Noraxon, USA) were placed over the tibia. The EMG signals were recorded in monopolar mode, bandpass filtered at 10-500 Hz, and digitized at a sampling rate of 2048 Hz using the multichannel HD-EMG acquisition system (EMG-Quattrocento, 400 channel EMG amplifier; OT Bioelettronica, Italy).

Data Analysis

Data were analyzed using MATLAB custom-written scripts (R2021a; The MathWorks, Natick, MA).

HD-EMG decomposition

The monopolar EMG signals were bandpass filtered between 20 and 500 Hz with a second-order Butterworth filter. After visual inspection, channels with low signal-to-noise ratio or artifacts were discarded. The HD-EMG signals were then decomposed into motor unit spike trains. We applied a

convolutive blind-source separation (Negro et al., 2016b). In short, the EMG signals were first extended and whitened. Thereafter, a fixed-point algorithm that maximized the sparsity was applied to identify the sources of the EMG signals, i.e., the motor unit spike trains. The spikes were separated from the noise using K-means classification and a second algorithm refined the estimation of the discharge times by minimizing the coefficient of variation of the inter-spike intervals while iteratively updating motor unit filters. This decomposition procedure has been validated using experimental and simulated signals (Negro et al., 2016b). After the automatic identification of the motor units, all of the motor unit spike trains were visually checked for false positives and false negatives (Del Vecchio et al., 2020; Hug et al., 2021b). Motor units with a pulse-to-noise ratio > 30 dB were retained for further analysis (Holobar et al., 2014).

Crosstalk and duplicates between motor units

We carefully checked all identified motor units for potential crosstalk units or duplicates, thus ensuring the uniqueness of each motor unit within the dataset (Hug et al., 2021a). To this end, we used the discharge times as a trigger to segment and average the HD-EMG signal over a window of 50 ms and identified the motor unit action potentials over the 64 electrodes of each grid. Then, we calculated the average peak-to-peak amplitude of the action potentials for each grid. We considered that a motor unit was falsely associated with a muscle due to crosstalk when the peak-to-peak amplitude was larger in a neighboring muscle than in the muscle of origin. On average, 2.6 ± 2.5 MUs were discarded from the analysis per participant. In addition, we verified that motor units identified from the grid located over the lateral and the medial parts of the SOL were not the same, i.e., duplicates. We considered duplicates as motor units that shared at least 30% of their discharge times with a tolerance of one data point (i.e., 0.5 ms; (Holobar et al., 2014)). At the end of these analyses, motor units identified over the lateral and medial parts of the SOL were pooled, with on average 0.7 ± 1.4 MUs discarded per participant.

Motor unit tracking

To assess whether a change in muscle length impacts the distribution of common synaptic inputs and motor unit behavior, we tracked the same motor units across conditions. Thus, we matched motor units using the unique spatiotemporal properties of motor unit action potentials within the

grids of electrodes (Martinez-Valdes et al., 2017; Vecchio and Farina, 2019; Oliveira and Negro, 2021). Specifically, the motor unit action potential shapes were identified using the spike-triggered averaging technique. As the position of the action potentials within the window may differ between motor units, we considered the local maxima, i.e., the action potential with the highest peak-to-peak amplitude within the grid, as the center of the 50 ms window. Finally, we concatenated the motor unit action potentials from the 64 channels, and we performed a 2D cross-correlation between motor units. Pairs with a correlation coefficient higher than 0.75 were considered as matches (Martinez-Valdes et al., 2017; Vecchio and Farina, 2019). The matches were visually checked to guarantee the similarity of the motor unit action potential shapes. Motor units were separately tracked between PF20° and PF0° and between DF20° and PF0°. Only motor units tracked across the three conditions were considered for the analyses. Average discharge rate over the torque plateau was estimated for all tracked motor units. All motor unit discharge characteristics were averaged across the three trapezoidal contractions.

Motor neuron synergies

We identified the common dynamics of motor unit smoothed discharge rates in Parts 1 and 2 using principal component analysis (PCA). The motivation behind this analysis was first to assess the ability of PCA to accurately identify the number of sources of common inputs, and then to estimate the minimal number of sources of common synaptic inputs, or motor neuron synergies, that can explain most of the variance of the smoothed discharge rate of the motor units from the triceps surae muscles. All motor units spike trains were converted into binary vectors where discharge times were equal to one. These binary signals were then convoluted with a 400-ms Hanning window, such that the correlation was calculated from the oscillations of the signal related to the fluctuation of force (i.e., < 2.5 Hz). It is noteworthy that focusing on the lowest bandwidth also limits the effect of the nonlinear relationship between the synaptic input and the output signal (Negro and Farina, 2012). These signals were high pass filtered to remove offsets and trends using a Butterworth filter 2nd order with a cut-off frequency of 0.75 Hz. Finally, we normalized the smoothed discharge rates between 0 and 1 to avoid any bias of the principal component analysis output due to differences in discharge rates between motor units and conditions.

Normalized smoothed discharge rates were then concatenated in a $n \times T$ matrix, where n is the number of tracked motor units and T the number of time samples. We applied PCA to this matrix

306 and identified n components ranked with the level of variance explained by each component. To
307 select the number of components of interest (i.e., motor neuron synergies), we fitted portions of the
308 curve of the variance explained with straight lines by iteratively decreasing the number of points
309 considered in the analysis. The number of components of interest was considered as the first data
310 point where the mean squared error of the fit falls under $5e^{-4}$ (Cheung et al., 2005; d'Avella et al.,
311 2011). In our study, this threshold was reached with two components for both the simulated and
312 experimental data. Then, we displayed two-dimensional biplots where x and y coordinates were
313 the weights of each motor unit in the two first components, and we applied k-means clustering on
314 these two-dimensional coordinates to assign each motor unit to a motor neuron synergy.
315
316 ***Pairs of motor units receiving common synaptic inputs***
317 For both Part 1 and Part 2, we estimated for each pair of motor units whether they received a
318 significant level of common synaptic input. To this end, we calculated the cross-correlation
319 between their smoothed discharge rates over a 10 s window that maximized the number of motor
320 units continuously firing during the plateaus of the submaximal contractions. The presence of
321 common synaptic input for each pair of motor units was estimated through the maximal cross-
322 correlation coefficient with a maximal lag of ± 100 ms (De Luca and Erim, 2002). We considered
323 that a pair of motor units received common synaptic input when the cross-correlation coefficient
324 was statistically significant (Rodriguez-Falces et al., 2017). Specifically, we defined a significance
325 threshold as the 95th percentile of the cross-correlation coefficient distribution generated with
326 resampled versions of all motor unit spike trains per participant and condition. To this end, we
327 generated random spike trains for each motor unit by bootstrapping the interspike intervals (random
328 sampling with replacement). This random spike train had the same number of spikes and the same
329 discharge rate (mean and standard deviation) as the original motor unit spike train. We repeated
330 this step four times per pair of motor units.
331
332 **Statistics**
333 All statistical analyses were performed with RStudio (USA). First, quantile-quantile plots and
334 histograms were displayed to check the normality of the data distribution. If the data were
335 determined not to be normal, they were transformed to remove the skew. All statistical analyses
336 were performed using linear mixed effect models implemented in the R package *lmerTest* with the

Kenward-Roger method to estimate the denominator degrees of freedom and the *p*-values. This method considers the dependence of data points (i.e., individual motor units) within each participant due to, e.g., common synaptic inputs. When necessary, multiple comparisons were performed using the R package *emmeans*, which adjusts the *p*-value using the Tukey method. The significance level was set at 0.05. Values are reported as mean ± standard deviation.

In Part 1, we assessed the ability of our methods to identify the number of synergies and classify the motor neurons according to the synaptic weights of the common inputs they receive. After verifying that the PCA accurately predicts the number of motor neuron synergies, we reported the percentage of motor neurons accurately assigned to the synergy with the highest synaptic weight using k-means clustering. Then, we reported the percentage of motor neurons belonging to the same synergy across simulations. Finally, we measured the level of common inputs between motor neurons having significant and non-significant cross correlation coefficients between their smoothed discharge rates across simulations. In this way, we wanted to quantify the minimal level of common input needed to reach the level of significance in the three conditions, and assess the maximal level of common input, if any, needed to have non-significant correlations in the three conditions.

In Part 2, we first compared MVC and torque RMSE using a linear mixed effects model with Condition (PF20°, PF0°, DF20°) as a fixed effect and Participant as a random effect. Motor unit average discharge rates were compared using a linear mixed effects model with Condition (PF20°, PF0°, DF20°) and Muscle (GL, GM, SOL) as fixed effects and Participant as a random effect.

Then, we used PCA to report the number of motor neuron synergies at each ankle angle for each participant. We classified each motor neuron using k-means clustering to associate them with one of the synergies. We reported the percentage of motor neurons belonging to the same synergy across the three angles. Finally, we assessed the level of common synaptic input to pairs of motor neurons from the same and different muscles using the cross-correlation coefficients between smoothed discharge rates. We used a linear mixed effects model to compare correlation coefficients with Muscle (GL, GM, SOL) and Condition (PF20°, PF0°, DF20°) as fixed effects and Participant as a random effect. We repeated the same analysis with Muscle pairs (GL-GM, GL-SOL, GM-SOL) and Condition (PF20°, PF0°, DF20°) as fixed effects and Participant as a random effect. The percentages of pairs of motor units with correlation coefficients above and below the significance

threshold at each ankle angle, as well as the proportion of pairs of motor units with significant or non-significant correlations across all angles were also reported.

Results

Part 1: Simulations

We first investigated the ability of our approach to capture the low dimensional control of motor neurons with PCA. The cumulative sum of the variance explained stopped increasing and reached a plateau with two components for all simulations (Fig. 2D). The value of variance explained with two components was 68.8, 70.9, and 72.1% for conditions CI#1 = CI#2, CI#1+ CI#2, and CI#1++ CI#2, respectively. Using k-means clustering, we accurately assigned 96%, 97%, and 94% of motor neurons to the synergy with the highest weight (Fig. 2A to 2C). On average, the motor neurons assigned to the wrong synergy received both sources of common inputs with balanced weights, ranging from 34%/66% to 49%/51%. Despite changes in the amplitude of CI#1 and CI#2 in the other simulations, 93% of motor neurons were assigned to the same synergy in all the simulations. Changes between synergies were observed for motor neurons receiving a relatively balanced ratio of CI#1 and CI#2, ranging from 34%/66% to 54%/46% (Fig. 2F).

We then performed cross-correlation between smoothed discharge rates of individual motor neurons with a significance threshold fixed at 0.29 (Fig. 2E). Correlation coefficients are displayed in Figure 2E according to the difference in ratio of common inputs, calculated as the differences of weights of CI#1 between the two motor neurons. For example, two motor neurons receiving 100% CI#1 / 0% CI#2 and 0% CI#1 / 100% CI#2 have a difference in ratio equal to 1. Motor neurons with a difference in ratio of common inputs of 0.29 ± 0.23, 0.30 ± 0.23, and 0.30 ± 0.23 had a significant correlation between their smoothed discharge rates in conditions CI#1 = CI#2, CI#1+ CI#2, and CI#1++ CI#2, respectively. Conversely, motor neurons with a difference in ratio of common inputs of 0.88 ± 0.13, had non-significant correlation between their smoothed discharge rates (Fig. 2E). 68.5% and 20.1% of the pairs of motor neurons had respectively significant or non-significant correlations between their smoothed discharge rates across the three simulations. Pairs of motor neurons with consistent non-significant correlations across simulations mostly received different inputs, with a difference in ratio of common inputs of 0.93 ± 0.09 (Fig. 2G). Pairs of motor neurons with consistent significant correlations across simulations mostly received the same inputs, with a difference in ratio of common inputs of 0.27 ± 0.21 (Fig. 2G). Pairs of motor neurons with changes in significance across simulations had differences in ratio of common inputs of 0.71 ± 0.12 (Fig. 2G). Together, these results showed that changes in assignment to synergies in the

PCA or in level of correlation in the cross-correlation analysis can be explained by the modulation of the amplitude of common synaptic inputs, despite fixed weights between simulations. It is noteworthy that motor neurons receiving low or high levels of the same sources of common inputs were always assigned to different synergies or always had the same level of correlation between the simulations. Motor neurons that did switch between synergies tended to have relatively balanced weights for each input.

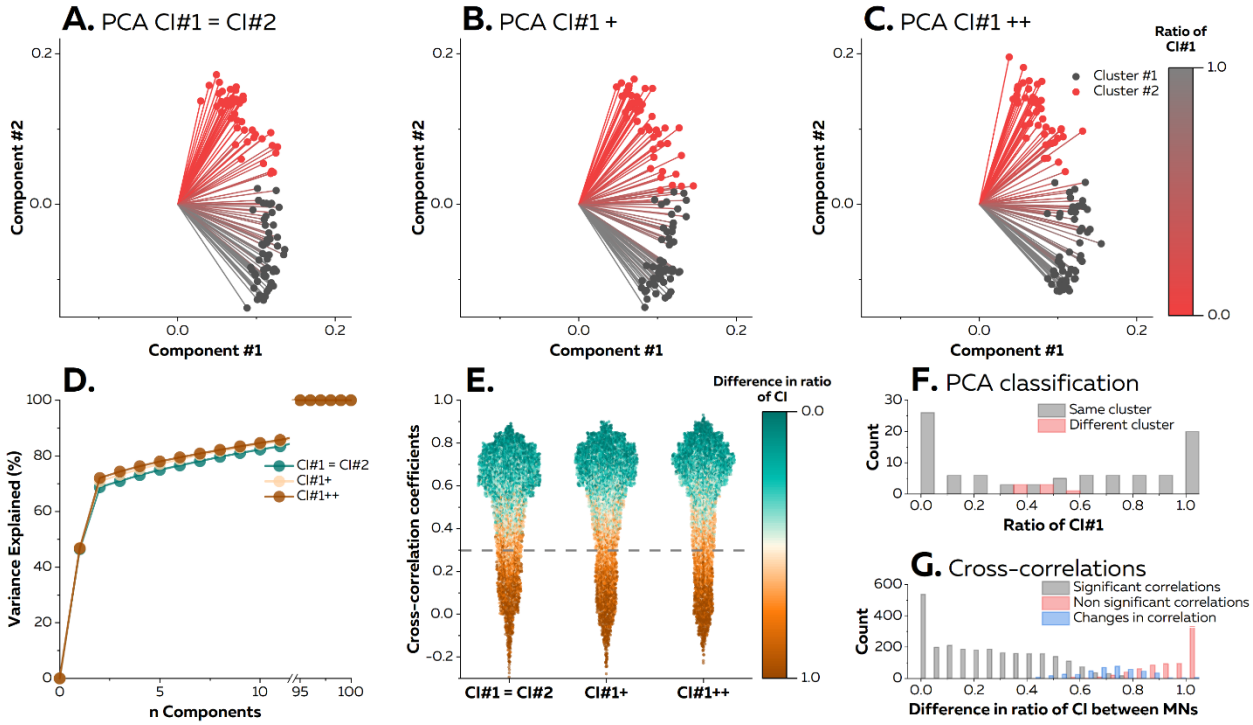

Figure 2: Simulation of a pool of motor neurons with two sources of common synaptic inputs. We simulated 100 motor neurons using an open-source model (Elias and Kohn, 2013). Each motor neuron received either 100% Common input #1 (CI#1, 20 motor neurons), 100% Common input #2 (CI#2, 20 motor neurons), or a ratio of CI#1 and CI#2 from 99% CI#1/ 1% CI#2 to 1% CI#1/ 99% CI#2 (60 motor neurons). We generated three simulations with different amplitudes of the common input #1 to mimic the divergent modulation of two separate sources of common synaptic inputs and to match the discharge rates experimentally observed during the plantarflexions. (A, B, C) We applied principal component analysis (PCA) and displayed the two-dimensional biplots based on the two main components. (D) Indeed, the cumulative sum of the variance explained reached a plateau with two components. We finally grouped these motor neurons into clusters using k-means clustering. Each line represents an individual motor neuron with the color depending on the ratio of CI#1 received by the motor neuron. The color of the scatter depends on the cluster. (E) Then, we estimated the level of common synaptic input for all pairs of motor neurons using cross-correlation analyses between individual motor neuron smoothed discharge rates. All correlations above 0.29 (dash grey line) were

significant. The color of scatters depends on the difference in the ratio of common input #1 between motor neurons in each pair. For example, two motor neurons receiving 100% CI#1 / 0% CI#2 and 0% CI#1 / 100% CI#2 have a difference in ratio equal to 1. (F, G) When we modulated the amplitude of CI#1 and CI#2, a portion of the pairs were assigned to a different cluster after PCA or had different levels of correlation. (F) Distribution of the ratio of CI#1 for each motor neuron staying in the same cluster or switching between clusters across simulations. (G) Distribution of difference in ratio for CI#1 for each pair of motor neurons with significant, non-significant, or different level of significance across simulations.

Part 2: Experiments

Torque

As expected, the MVC torque was significantly different between conditions ($F = 36.94$, $p < 0.001$), with MVC torque at PF20° (383.4 ± 225.4 N.m) being significantly lower than that at PF0° (715.7 ± 354.8 N.m, $p < 0.001$) and DF20° (790.0 ± 448.2 N.m, $p < 0.001$). There was no difference between PF0° and DF20° ($p = 0.892$). The RMSE was not significantly different between conditions ($F = 2.73$, $p = 0.082$), meaning that the target torque was matched with similar accuracy across conditions.

Motor unit discharge characteristics

A total of 595, 613, and 471 motor units were identified at PF20°, PF0°, and DF20°, respectively. They had an average pulse-to-noise ratio of 33.3 ± 2.6 dB. 170 motor units (30.4%) were tracked over the three conditions, with 32, 56, and 82 motor units for the GL, GM, and SOL, respectively. It is noteworthy that four participants were excluded from the analyses, as no motor units could be tracked across conditions, and thus data are reported for the 12 remaining participants. We first compared the discharge characteristics of these tracked motor units (Fig. 3). When considering the average discharge rates, significant effects of Condition ($F = 19.43$, $p < 0.001$), Muscle ($F = 28.30$, $p < 0.001$), and an interaction Condition × Muscle ($F = 3.61$, $p = 0.006$) were observed. The average discharge rate of motor units from the GL was significantly lower at DF20° (7.6 ± 2.1 pps) than at PF20° (9.8 ± 2.5 pps). No significant differences were observed for other angles or muscles (all $p > 0.114$).

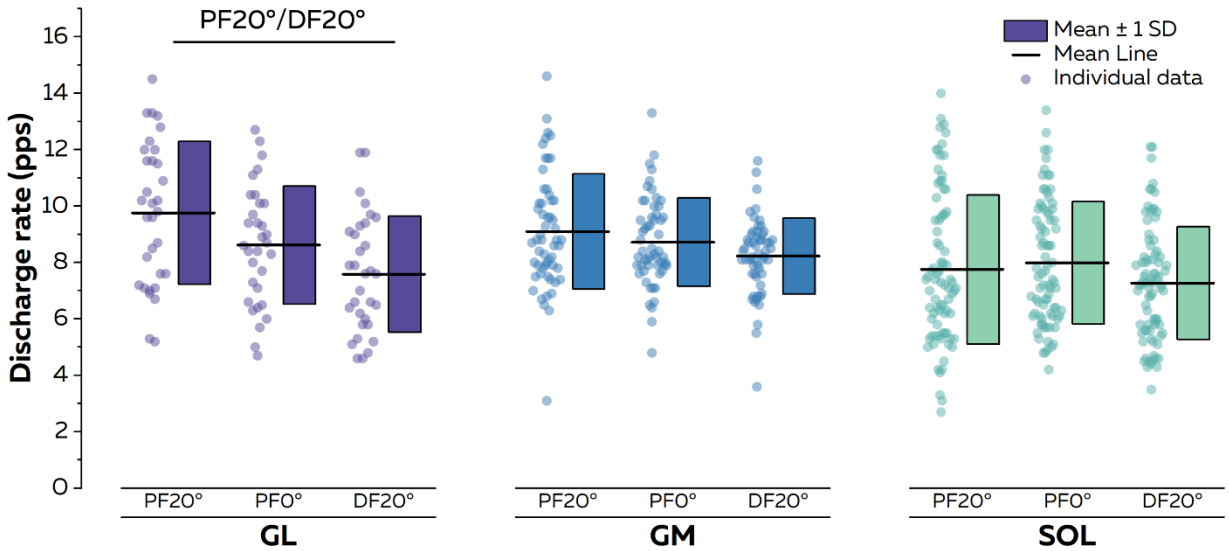

Figure 3: Motor unit discharge characteristics. We compared the discharge characteristics of all tracked motor units. The average discharge rate was estimated after smoothing instantaneous discharge rates with a 1s Hanning window over the plateau. Each scatter represents an individual motor unit. The horizontal lines on top of the plots depict the significant statistical differences with a $p < 0.05$. For the sake of clarity, we only reported the differences within muscles. GL: Gastrocnemius lateralis; GM: Gastrocnemius medialis; SOL: Soleus.

Motor neuron synergies

The motor neuron synergy analysis was performed for participants with more than nine tracked motor units across the three conditions (n = 7; 15 ± 7 MUs). PCA was performed on the normalized smoothed discharge rates. We first intended to identify the minimal number of sources of common synaptic inputs, or motor neuron synergies, that explained most of the variance of the smoothed discharge rates. To this end, we used mean-square error to determine the number of components where the cumulative sum of the variance explained reaches a plateau (Cheung et al., 2005; d'Avella et al., 2011) and found on average two motor neuron synergies (Fig. 4). The value of variance explained with two components was 57.0, 57.4, and 57.9% for conditions PF20°, PF0°, and DF20°, respectively. Then, two-dimensional biplots with the weight of each motor unit in the two motor neuron synergies were displayed. Motor units were clustered based on their coordinates within the two-dimensional biplots using K-means classification (Fig. 4). It is noteworthy that 40.5% of the clusters (n = 17) grouped motor units from different muscles, indicating that the motor neuron synergies spanned across muscles. In addition, motor units from GL and GM were only grouped in 7.1% of the clusters (n = 3). When considering motor units from the same muscles, motor units from either GL or GM were separated between two clusters in 1 out of 21 biplots

reported here (3 conditions × 7 participants), while motor units from SOL were separated between two clusters in 12 out of 21 biplots, indicating that the individual muscles were not necessarily the functional unit of control. We further investigated the distribution of common inputs across conditions by reporting the ratio of motor units that belonged to the same clusters. 74.0% of the motor units belonged to the same clusters across all the conditions, despite changes in the mechanical constraints of the task.

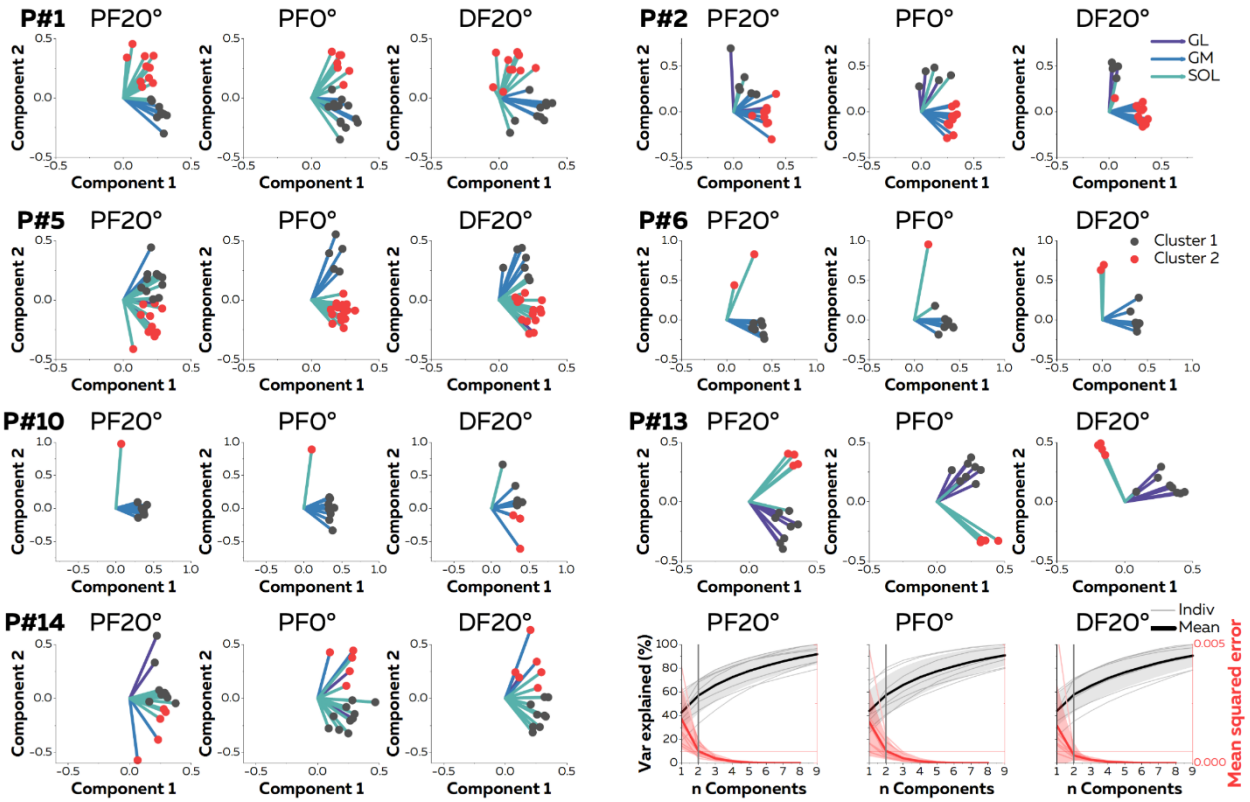

Figure 4: Biplots of motor unit weights from the two motor neuron synergies in seven representative participants. We applied principal component analysis on normalized smoothed discharge rates concatenated in a matrix per participant. The identified components were ranked based on the variance they explained (lowest panels on the right corner), with two components sufficient such that the variance explained reached a plateau. Then, we displayed two dimensional biplots where coordinates of each motor unit are the weights of the two motor neuron synergies. We finally grouped these motor units into clusters using k-means clustering. Each line represents an individual motor unit. The color of the scatter depends on the cluster. GL: Gastrocnemius lateralis; GM: Gastrocnemius medialis; SOL: Soleus The lower right panels display the cumulative sum of variance explained by each component and the mean squared error used to identify the number of motor neuron synergies.

Pairs of motor units receiving common synaptic inputs

We analyzed the correlation between 812 pairs of matched motor unit activities. Specifically, we had 32, 134, and 237 pairs of motor units for GL, GM, and SOL, respectively, and 57, 119, and 233 pairs of motor units for GL-GM, GL-SOL, and GM-SOL, respectively. We first compared the degree of common synaptic input between motor units innervating the same muscle (i.e., GL, GM, SOL on Fig. 5A). The coefficients of correlation were significantly different between Conditions ($F = 4.06$, $p = 0.018$) and Muscles ($F = 52.09$, $p < 0.001$) with a significant interaction ($F = 18.85$, $p < 0.001$). Specifically, the coefficients of correlation for pairs of motor units within the GM and SOL were significantly lower for PF0° ($p < 0.001$) and DF20° ($p < 0.001$) compared to PF20° while coefficients for the GL were not significantly different. We then compared the correlations between motor units from different muscles (i.e., GL-GM, GL-SOL, GM-SOL on Fig. 5A). The coefficients of correlation were significantly different between Conditions ($F = 37.28$, $p < 0.001$) and Muscle Pairs ($F = 20.86$, $p < 0.001$), with a significant interaction ($F = 2.81$, $p = 0.025$). Specifically, the coefficients of correlation for pairs of motor units between GL-SOL and GM-SOL were significantly lower for PF0° ($p < 0.001$) and PF20° ($p < 0.001$) compared to DF20° while coefficients for the GL-GM were not significantly different across conditions. The ratio of pairs of motor units with significant correlations across all conditions reached an average of 84.4%, 85.3%, and 67.4% for GL, GM, and SOL, respectively (Fig. 5B). The ratio of pairs of motor units with significant correlations across all conditions reached an average of 27.5%, 56.3%, and 37.9% for GL-GM, GL-SOL, and GM-SOL, respectively.

We then compared the distribution of common synaptic input across conditions by calculating the ratio of pairs of motor units with the same level of correlation (either significant or non-significant correlations) across the three angles (Fig. 5C). The rest of the motor units switched between significant and non-significant correlations across conditions. When considering pairs of motor units from the same muscle, 0%, 0%, and 5.9% of pairs of motor units had a non-significant level of correlation across all conditions for GL, GM, and SOL, respectively, while 59.3%, 59.7%, and 32.1% of pairs of motor units had a significant level of correlation across angles for GL, GM, and SOL, respectively (Fig. 5C). When considering pairs of motor units from different muscles, 50.8%, 15.1%, and 22.3% of pairs of motor units had a non-significant level of correlation across angles for GL-GM, GL-SOL, and GM-SOL, respectively, while 10.5%, 28.6%, and 7.7% of pairs of motor units had a significant level of correlation across angles for GL-GM, GL-SOL, and GM-SOL,

respectively (Fig. 5C). It is noteworthy that we failed to identify a significant level of correlation in a non-negligible percentage of pairs of motor units from the same muscle. Conversely, some pairs of motor units from different muscles, most notably GL-SOL and GM-SOL, exhibited significant correlations, supporting the findings from the PCA of two common inputs. Moreover, the level of correlation appears to change for a significant percentage of pairs of motor units, which may reflect how motor units receive two sources of common inputs.

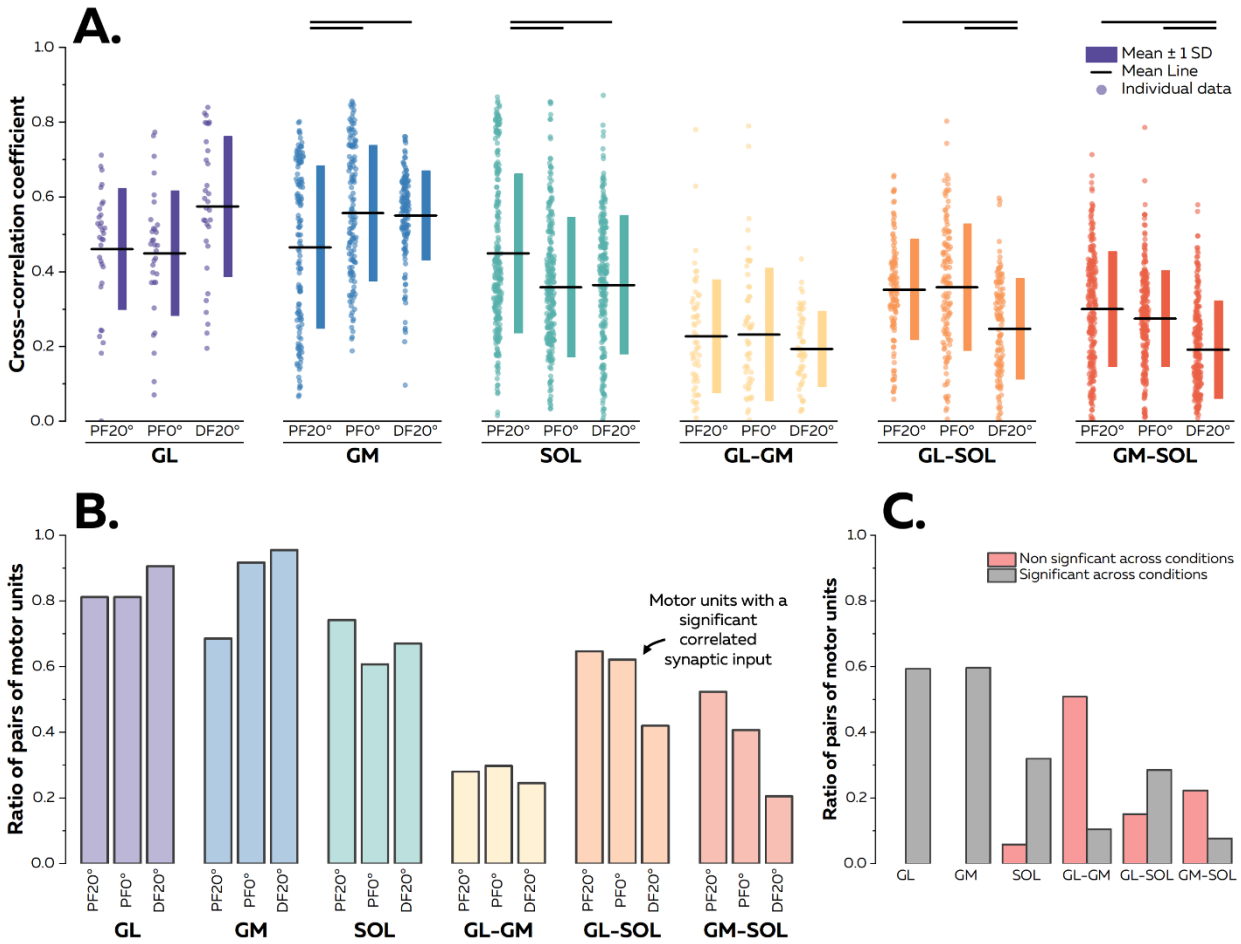

Figure 5: Common synaptic inputs to pairs of motor units. We estimated the level of common synaptic input for all pairs of motor units from the same and different muscles using cross-correlation analyses between individual motor units smoothed discharge rates. (A) We first compared the level of correlation for each individual muscle and pairs of muscles. Each scatter represents a pair of motor units. The horizontal lines on top of the plots depict the significant statistical differences with a $p < 0.05$. For the sake of clarity, we only reported the differences for the interaction. (B) We calculated the ratio of pairs of motor units with significant correlations for each individual muscle and pairs of muscles. (C) To compare the changes in common synaptic input to pairs of motor units across conditions, we calculated

the ratio of pairs of motor units with non-significant and significant level of correlation across angles. GL: Gastrocnemius lateralis; GM: Gastrocnemius medialis; SOL: Soleus.

Discussion

This study aimed to identify and track synergies at the motor neuron level across conditions with different mechanical constraints to test their robustness. In the first part, we used simulated signals to estimate the sensitivity of our methods (i.e., principal component analysis and correlation of smoothed discharge rates) to identify the number of sources of common inputs and their distribution across motor neurons with various amplitudes of synaptic inputs. We found that PCA can accurately classify motor units according to the sources of common input they receive. Only motor units that received the two common inputs with balanced weights (i.e., 34%/66% to 54%/46%) switched between clusters across conditions. Moreover, cross-correlations can accurately identify pairs of motor neurons receiving or not receiving a significant level of common inputs. This approach was then applied to experimental data. We identified two main sources of common input driving motor neurons innervating the GL, GM, and SOL, with one common input mainly distributed between GL and SOL motor units and another common input mainly distributed between GM and SOL motor units. 74.0% of the identified motor units belonged to the same motor neuron synergy across ankle angles. Moreover, cross-correlation analysis revealed that only 13.9% of pairs of motor neurons had a non-significant level of correlation across angles, suggesting the large presence of common inputs across motor units. It is noteworthy that a majority of the pairs grouping motor units from the GL and GM had non-significant correlations (50.8%). Overall, these results highlight a modular organization of the control of motor neurons innervating the triceps surae muscles with a reduced dimensionality.

Methodological considerations

Our experiment is a first step toward the demonstration of the modular organization of the neural control of motor neurons across tasks with different mechanical constraints. As previously noted, the assessment of motor neuron synergies across tasks required the tracking of the same motor units. To this end, we matched the unique spatiotemporal properties of the motor unit action potential shapes over the grids of electrodes between trials (Martinez-Valdes et al., 2017; Vecchio and Farina, 2019; Oliveira and Negro, 2021). As changes in ankle position inevitably impacted the geometry of the volume conductor, the shapes of action potentials over the skin slightly varied across conditions. Although we successfully tracked a significant number of motor units (30.4%),

571 there was a significant reduction in the motor unit sample that could be analyzed across tasks. The
572 recent development of intramuscular thin-film arrays with a high density of electrodes (Muceli et
573 al., 2022) may open new perspectives to accomplish this goal as these electrodes may be less
574 affected by the changes in muscle geometry. Additionally, Oliveira and Negro (2021) have
575 demonstrated the ability to decompose HD-EMG signals during slow dynamic contractions, which
576 may provide opportunities to show the robustness of motor neuron synergies during more natural
577 behaviors.

578 Despite the above-mentioned methodological limitations and perspectives, studying the robustness
579 of the distribution of common inputs driving the triceps surae muscles during plantarflexions
580 performed at multiple angles has revealed very relevant results. Previous works highlighted a
581 differential change in neural drive between the three heads of the triceps surae during sustained
582 contractions and in response to the alteration of force generating capacity during an ankle rotation
583 (Lacourpaille et al., 2017; Hug et al., 2021a; Rossato et al., 2022). Additionally, Marshall et al.
584 (2022) have recently shown that the covariation of motor unit discharge rates and their recruitment
585 order may change between short and long muscle lengths. Both results suggested that the central
586 nervous system could drive these muscles with more than one common input, even during a task
587 with one degree of freedom. Our results supported this hypothesis, with the identification of two
588 sources of common inputs driving the triceps surae muscles. However, whether the distribution of
589 common inputs to motor units is robust across muscle lengths was unknown. In this study we
590 further described the distribution of these common inputs within and between these muscles,
591 showing a flexible combination of these inputs across motor units.

592

593 **Distribution of common inputs to modulate muscle force**

594 Numerous works have shown that most of the motor units from the same muscle display common
595 variations of their discharge rate, which is necessary to modulate force during isometric
596 contractions (Farina et al., 2014b; Farina and Negro, 2015; Enoka and Farina, 2021). These
597 common fluctuations depend on the modulation of correlated synaptic inputs, or common inputs,
598 received by all of these motor units (Negro et al., 2009; Farina et al., 2014a; Farina et al., 2014b;
599 Farina and Negro, 2015; Feeney et al., 2018). In line with these studies, we observed that only 0%,
600 0%, and 5.9% of pairs of motor units had a non-significant level of correlation across angles for

601 GL, GM, and SOL, respectively (Fig. 5C). The level of common input to motor neurons from either
602 GL or GM was particularly high, with a ratio of pairs with significant correlation reaching 84.4%
603 and 85.3% for GL and GM, respectively, and only one condition where motor units from either GL
604 or GM were separated between two clusters after PCA (Fig. 3). On the contrary, the degree of
605 common input between motor units from GL and GM was lower than for the other pairs of muscles,
606 with a ratio of pairs of motor units with significant correlation at 27.5% across conditions and only
607 7.1% of the clusters grouping motor units from GL and GM (n=3; Fig. 3). This is in agreement
608 with previous works that used methods at the muscle level, such as intramuscular coherence (Hug
609 et al., 2021a; Rossato et al., 2022) or PCA (Mazzo et al., 2022), to assess the common fluctuations
610 of motor unit discharge rates in the triceps surae muscles. Motor units from the SOL appear to have
611 lower correlated fluctuations in discharge rates than GL and GM. This may be a result of the
612 geometry and compartmentalization of this muscle (Bolsterlee et al., 2018), requiring multiple
613 sources of common input to drive multiple functions (Segal et al., 1991; English et al., 1993). Such
614 results have been observed in muscles from the forearm with multiple compartments and tendons
615 (Keen and Fuglevand, 2004; Hockensmith et al., 2005; McIsaac and Fuglevand, 2007).
616 Alternatively, one may consider the absence of correlation as a result of different non-linear
617 inputs/outputs functions for each motor neuron due to the activation of persistent inward currents
618 (Heckman et al., 2008; Binder et al., 2020). However, we focused our analysis on oscillations with
619 frequencies below the averaged motor unit discharge rates, which are less affected by these non-
620 linear transformations of synaptic inputs (Negro and Farina, 2012). Therefore, we are confident
621 that this absence of significant correlation identifies motor units receiving independent sources of
622 common input, as suggested for motor units from muscles of the upper (Madarshahian et al., 2020;
623 Marshall et al., 2022) and lower limbs (Del Vecchio et al., 2022; Hug et al., 2022b).

624

625 **From muscle to motor neuron synergies**

626 The fact that the central nervous system may group motor units from synergistic muscles to reduce
627 the dimensionality of the neural control of movements has been supported for decades by the theory
628 of muscle synergies (Tresch and Jarc, 2009; Dominici et al., 2011; Bizzi and Cheung, 2013; Ting
629 et al., 2015; Takei et al., 2017). Of note, these synergies have been mostly described at the muscle
630 level, assuming that all motor neurons innervating each muscle would receive the same common

inputs (Cheung and Seki, 2021). However, several studies have highlighted higher correlations between the firing activities of motor units from synergistic muscles than from the same muscle (Keen and Fuglevand, 2004; McIsaac and Fuglevand, 2007; Del Vecchio et al., 2022; Hug et al., 2022b). For this reason, previous studies have proposed to take advantage of the large sampling of motor unit activity from decomposed HD-EMG signals to revisit muscle synergies at the motor neuron level, i.e., identifying motor neuron synergies (Madarshahian et al., 2020; Tanzarella et al., 2021; Del Vecchio et al., 2022; Hug et al., 2022a; Hug et al., 2022b). Here, we found two main motor neuron synergies mostly grouping motor units from GL/SOL and GM/SOL. Specifically, two components were identified through PCA and motor units from GL and GM were grouped into 7.1% of the clusters (n=3). The relative lower ratio of pairs of motor units from GL and GM receiving common inputs is consistent with previous works highlighting non-significant coherence between these two muscles (Hug et al., 2021a; Rossato et al., 2022). Conversely, Gibbs et al. (1995) reported that motor units from the gastrocnemius and the soleus muscles did receive common inputs, consistent with our results.

The results of our study supported three of the hypotheses postulated by Hug et al (2022a) within the motor neuron synergies framework, namely that during movement 1) motor neurons are grouped into functional groups (clusters) based on the common inputs they receive; 2) clusters may significantly differ from the classical definition of motor neuron pools, such that clusters of motor neurons may span across muscles (i.e., GL and SOL, GM and SOL) and/or involve only a portion of a muscle (i.e., SOL); and 3) clusters represent functional modules used by the central nervous system to reduce the dimensionality of control. The latter observation is the main novelty of our study. Previous studies identified motor neuron synergies during isometric contractions performed at a single joint angle (Madarshahian et al., 2020; Del Vecchio et al., 2022; Hug et al., 2022b) and, therefore, did not demonstrate their invariance across tasks, which is needed to reduce the computational burden of movement control (d'Avella et al., 2003; d'Avella and Bizzi, 2005). To this end, we tested the robustness of motor neuron clusters (synergies) across ankle angles, and 74.0% of the tracked motor neurons were assigned to the same synergies across the conditions (Fig. 4). Our simulations showed that motor neurons switching between motor neuron synergies across angles may receive the two sources of common inputs with relatively balanced weights (i.e., 34%/66% to 49%/51 in the simulation). The different changes in the amplitude of each source of common input may then impact the level of covariation between motor unit discharge rates across

angles. This would explain the large number of pairs of motor units switching from significant to non-significant correlations across angles and why PCA cannot accurately classify these motor units in the same synergy across conditions. To support this idea, divergent variations in neural drive to the triceps surae muscles have been indirectly observed while the position of the ankle changed during isometric contractions (Huang et al., 2016; Cibulka et al., 2017; Lacourpaille et al., 2017; Hug et al., 2021a). Overall, we suggest that the distribution of common inputs across motor units is indeed robust across tasks with some changes in the clustering due to divergent changes in the amplitude of common inputs to motor neurons receiving the two inputs.

The concept of combining motor neuron synergies to generate movements may bridge the gap between studies supporting modular control and flexible control of motor units. Proponents of flexible control of motor units suggest that motor units from the same muscle may receive independent inputs instead of one common input, explaining changes in recruitment order between the same motor units across multiple tasks (Basmajian, 1963; Formento et al., 2021; Marshall et al., 2022). We show here that most of the motor units from the triceps surae muscles may receive two sources of common inputs. The combination of these two independent inputs may explain why previous works reported changes in recruitment strategies between motor units from the same muscle while changing the mechanical constraints of the task (Desmedt and Godaux, 1981; ter Haar Romeny et al., 1984; Herrmann and Flanders, 1998; Marshall et al., 2022).

Neural structures that shape the modular control of calf muscles

These results suggest that the neural control of movements may be hierarchically organized, where motor neuron synergies are controlled instead of individual motor neurons (Loeb et al., 1999). Thus, spinal circuits involving premotor neurons and interneurons may span across motor nuclei to transmit these correlated inputs to synergist muscles (Levine et al., 2014; Takei et al., 2017; Ronzano et al., 2021). However, as motor neurons are the final common pathways where inputs from supraspinal centers and afferent fibers converge, we cannot make any inference about the origin of the correlated inputs though several candidates exist. For example, previous works found that the stimulation of the motor cortex (Overduin et al., 2012) or premotor neurons in the spinal cord (Takei et al., 2017) evoked synergies comparable to those observed during natural behaviors. Additionally, Cheung et al. (2005) observed similar synergies in animals with intact and

692 deafferented nervous systems, suggesting that the activation of synergies would mostly be a
693 feedforward process. Alternatively, others proposed that the correlated activity between synergistic
694 muscles may aim to regulate mechanical features such as internal joint stress, thus emphasizing the
695 key role of sensory feedback (Alessandro et al., 2020). This could also be the case in our study as
696 the variation of ankle angles undoubtedly impacts the behavior of motor neurons during
697 plantarflexions (Kennedy and Cresswell, 2001; Trypidakis et al., 2021). Additionally, our two
698 synergies may allow the central nervous system to tune the behavior of the lateral and medial
699 portions of the calf muscles to stabilize the foot producing plantarflexion in the frontal plane (Lee
700 and Piazza, 2008), thus limiting the strain and the stress of the ankle joint. Overall, future work is
701 needed to identify the neural bases of correlated inputs to motor neurons during voluntary
702 movements (Cheung and Seki, 2021).

703

704 # Conclusion

705 Our results support the concept that the central nervous system may flexibly combine modular
706 structures, i.e., motor neuron synergies, to produce movements. Specifically, we identified two
707 motor neuron synergies grouping motor units from GL/SOL and GM/SOL during plantarflexion
708 performed at multiple ankle angles. Importantly, we found that the structure of these motor
709 synergies was invariant across conditions despite the variation of mechanical constraints with some
710 level of flexibility that may be accounted for by modulated magnitude of common inputs. This
711 provides a novel observation that significantly contributes to demonstrate the functional relevance
712 of such modular structures to generate movements.

713

References

Alessandro C, Barroso FO, Prashara A, Tentler DP, Yeh HY, Tresch MC (2020) Coordination amongst quadriceps muscles suggests neural regulation of internal joint stresses, not simplification of task performance. Proc Natl Acad Sci U S A:201916578.

Basmajian JV (1963) Control and training of individual motor units. Science 141:440-441.

Binder MD, Powers RK, Heckman CJ (2020) Nonlinear Input-Output Functions of Motoneurons. Physiology (Bethesda) 35:31-39.

Bizzi E, Cheung VC (2013) The neural origin of muscle synergies. Front Comput Neurosci 7:51.

Bolsterlee B, Finni T, D'Souza A, Eguchi J, Clarke EC, Herbert RD (2018) Three-dimensional architecture of the whole human soleus muscle in vivo. PeerJ 6:e4610.

Cheung VC, d'Avella A, Tresch MC, Bizzi E (2005) Central and sensory contributions to the activation and organization of muscle synergies during natural motor behaviors. J Neurosci 25:6419-6434.

Cheung VCK, Seki K (2021) Approaches to Revealing the Neural Basis of Muscle Synergies: A Review and A Critique. J Neurophysiol.

Christakos CN, Papadimitriou NA, Erimaki S (2006) Parallel neuronal mechanisms underlying physiological force tremor in steady muscle contractions of humans. J Neurophysiol 95:53-66.

Cibulka M, Wenthe A, Boyle Z, Callier D, Schwerdt A, Jarman D, Strube MJ (2017) VARIATION IN MEDIAL AND LATERAL GASTROCNEMIUS MUSCLE ACTIVITY WITH FOOT POSITION. International journal of sports physical therapy 12:233-241.

Cisi RR, Kohn AF (2008) Simulation system of spinal cord motor nuclei and associated nerves and muscles, in a Web-based architecture. Journal of computational neuroscience 25:520-542.

d'Avella A, Bizzi E (2005) Shared and specific muscle synergies in natural motor behaviors. Proc Natl Acad Sci U S A 102:3076-3081.

d'Avella A, Saltiel P, Bizzi E (2003) Combinations of muscle synergies in the construction of a natural motor behavior. Nat Neurosci 6:300-308.

d'Avella A, Portone A, Lacquaniti F (2011) Superposition and modulation of muscle synergies for reaching in response to a change in target location. J Neurophysiol 106:2796-2812.

De Luca CJ, Erim Z (2002) Common drive in motor units of a synergistic muscle pair. J Neurophysiol 87:2200-2204.

Del Vecchio A, Holobar A, Falla D, Felici F, Enoka RM, Farina D (2020) Tutorial: Analysis of motor unit discharge characteristics from high-density surface EMG signals. Journal of Electromyography and Kinesiology:102426.

Del Vecchio A, Germer C, Kinfe TM, Nuccio S, Hug F, Eskofier B, Farina D, Enoka RM (2022) Common synaptic inputs are not distributed homogeneously among the motor neurons that innervate synergistic muscles. bioRxiv:2022.2001.2023.477379.

Desmedt HE, Godaux E (1981) Spinal motoneuron recruitment in man: rank deordering with direction but not with speed of voluntary movement. Science 214:933-936.

Dominici N, Ivanenko YP, Cappellini G, d'Avella A, Mondi V, Cicchese M, Fabiano A, Silei T, Di Paolo A, Giannini C, Poppele RE, Lacquaniti F (2011) Locomotor primitives in newborn babies and their development. Science 334:997-999.

Elias LA, Kohn AF (2013) Individual and collective properties of computationally efficient motoneuron models of types S and F with active dendrites. Neurocomputing 99:521-533.

English AW, Wolf SL, Segal RL (1993) Compartmentalization of muscles and their motor nuclei: the partitioning hypothesis. Physical therapy 73:857-867.

Enoka RM, Farina D (2021) Force Steadiness: From Motor Units to Voluntary Actions. Physiology (Bethesda) 36:114-130.

Farina D, Negro F (2015) Common synaptic input to motor neurons, motor unit synchronization, and force control. Exerc Sport Sci Rev 43:23-33.

Farina D, Holobar A (2016) Characterization of Human Motor Units From Surface EMG Decomposition. Proceedings of the IEEE 104:353-373.

Farina D, Merletti R, Enoka RM (2014a) The extraction of neural strategies from the surface EMG: an update. J Appl Physiol (1985) 117:1215-1230.

Farina D, Negro F, Dideriksen JL (2014b) The effective neural drive to muscles is the common synaptic input to motor neurons. J Physiol 592:3427-3441.

Feeney DF, Mani D, Enoka RM (2018) Variability in common synaptic input to motor neurons modulates both force steadiness and pegboard time in young and older adults. J Physiol 596:3793-3806.

Formento E, Botros P, Carmena JM (2021) A non-invasive brain-machine interface via independent control of individual motor units. bioRxiv:2021.2003.2022.436518.

Gibbs J, Harrison LM, Stephens JA (1995) Organization of inputs to motoneurone pools in man. J Physiol 485 (Pt 1):245-256.

Glover IS, Baker SN (2022) Both Corticospinal and Reticulospinal Tracts Control Force of Contraction. J Neurosci.

Heckman CJ, Enoka RM (2012) Motor unit. Compr Physiol 2:2629-2682.

Heckman CJ, Johnson M, Mottram C, Schuster J (2008) Persistent inward currents in spinal motoneurons and their influence on human motoneuron firing patterns. Neuroscientist 14:264-275.

Herrmann U, Flanders M (1998) Directional tuning of single motor units. J Neurosci 18:8402-8416.

Hockensmith GB, Lowell SY, Fuglevand AJ (2005) Common input across motor nuclei mediating precision grip in humans. J Neurosci 25:4560-4564.

Holobar A, Minetto MA, Farina D (2014) Accurate identification of motor unit discharge patterns from high-density surface EMG and validation with a novel signal-based performance metric. J Neural Eng 11:016008.

Huang C, Chen X, Cao S, Zhang X (2016) Muscle-tendon units localization and activation level analysis based on high-density surface EMG array and NMF algorithm. J Neural Eng 13:066001.

Hug F, Avrillon S, Ibáñez J, Farina D (2022a) Common Synaptic Input, Synergies, and Size Principle: Control of Spinal Motor Neurons for Movement Generation. In, p arXiv:2208.02818.

Hug F, Del Vecchio A, Avrillon S, Farina D, Tucker K (2021a) Muscles from the same muscle group do not necessarily share common drive: evidence from the human triceps surae. J Appl Physiol (1985) 130:342-354.

Hug F, Avrillon S, Sarcher A, Del Vecchio A, Farina D (2022b) Correlation networks of spinal motor neurons that innervate lower limb muscles during a multi-joint isometric task. J Physiol.

Hug F, Avrillon S, Del Vecchio A, Casolo A, Ibanez J, Nuccio S, Rossato J, Holobar A, Farina D (2021b) Analysis of motor unit spike trains estimated from high-density surface electromyography is highly reliable across operators. J Electromyogr Kinesiol 58:102548.

Keen DA, Fuglevand AJ (2004) Common input to motor neurons innervating the same and different compartments of the human extensor digitorum muscle. J Neurophysiol 91:57-62.
Kennedy PM, Cresswell AG (2001) The effect of muscle length on motor-unit recruitment during isometric plantar flexion in humans. Exp Brain Res 137:58-64.
Lacourpaille L, Nordez A, Hug F (2017) The nervous system does not compensate for an acute change in the balance of passive force between synergist muscles. J Exp Biol.
Laine CM, Yavuz SU, Farina D (2014) Task-related changes in sensorimotor integration influence the common synaptic input to motor neurones. Acta Physiol (Oxf) 211:229-239.
Laine CM, Martinez-Valdes E, Falla D, Mayer F, Farina D (2015) Motor Neuron Pools of Synergistic Thigh Muscles Share Most of Their Synaptic Input. J Neurosci 35:12207-12216.
Lee SS, Piazza SJ (2008) Inversion-eversion moment arms of gastrocnemius and tibialis anterior measured in vivo. J Biomech 41:3366-3370.
Lemon RN (2008) Descending pathways in motor control. Annual review of neuroscience 31:195-218.
Levine AJ, Hinckley CA, Hilde KL, Driscoll SP, Poon TH, Montgomery JM, Pfaff SL (2014) Identification of a cellular node for motor control pathways. Nat Neurosci 17:586-593.
Loeb GE, Brown IE, Cheng EJ (1999) A hierarchical foundation for models of sensorimotor control. Exp Brain Res 126:1-18.
Madarshahian S, Letizi J, Latash ML (2020) Synergic control of a single muscle: The example of flexor digitorum superficialis. J Physiol.
Marshall NJ, Glaser JI, Trautmann EM, Amematsro EA, Perkins SM, Shadlen MN, Abbott LF, Cunningham JP, Churchland MM (2022) Flexible neural control of motor units. Nat Neurosci:2021.2005.2005.442653.
Martinez-Valdes E, Negro F, Laine CM, Falla D, Mayer F, Farina D (2017) Tracking motor units longitudinally across experimental sessions with high-density surface electromyography. J Physiol 595:1479-1496.
Mazzo MR, Holobar A, Enoka RM (2022) Association between effective neural drive to the triceps surae and fluctuations in plantar-flexion torque during submaximal isometric contractions. Exp Physiol 107:489-507.
McIsaac TL, Fuglevand AJ (2007) Motor-unit synchrony within and across compartments of the human flexor digitorum superficialis. J Neurophysiol 97:550-556.
Muceli S, Poppendieck W, Holobar A, Gandevia S, Liebetanz D, Farina D (2022) ACCURATE DECODING OF THE SPINAL CORD OUTPUT IN HUMANS WITH IMPLANTED HIGH-DENSITY ELECTRODE ARRAYS. bioRxiv:2022.2001.2029.478247.
Negro F, Farina D (2012) Factors influencing the estimates of correlation between motor unit activities in humans. PLoS One 7:e44894.
Negro F, Holobar A, Farina D (2009) Fluctuations in isometric muscle force can be described by one linear projection of low-frequency components of motor unit discharge rates. J Physiol 587:5925-5938.
Negro F, Yavuz US, Farina D (2016a) The human motor neuron pools receive a dominant slow-varying common synaptic input. J Physiol 594:5491-5505.
Negro F, Muceli S, Castronovo AM, Holobar A, Farina D (2016b) Multi-channel intramuscular and surface EMG decomposition by convolutive blind source separation. J Neural Eng 13:026027.
Oliveira AS, Negro F (2021) Neural control of matched motor units during muscle shortening and lengthening at increasing velocities. J Appl Physiol (1985) 130:1798-1813.

Overduin SA, d'Avella A, Carmena JM, Bizzi E (2012) Microstimulation activates a handful of muscle synergies. Neuron 76:1071-1077.

Rodriguez-Falces J, Negro F, Farina D (2017) Correlation between discharge timings of pairs of motor units reveals the presence but not the proportion of common synaptic input to motor neurons. J Neurophysiol 117:1749-1760.

Ronzano R, Lancelin C, Bhumbra GS, Brownstone RM, Beato M (2021) Proximal and distal spinal neurons innervating multiple synergist and antagonist motor pools. Elife 10.

Rossato J, Tucker KJ, Avrillon S, Lacourpaille L, Holobar A, Hug F (2022) Less common synaptic input between muscles from the same group allows for more flexible coordination strategies during a fatiguing task. J Neurophysiol.

Segal RL, Wolf SL, DeCamp MJ, Chopp MT, English AW (1991) Anatomical partitioning of three multiarticular human muscles. Acta Anat (Basel) 142:261-266.

Takei T, Confais J, Tomatsu S, Oya T, Seki K (2017) Neural basis for hand muscle synergies in the primate spinal cord. Proc Natl Acad Sci U S A 114:8643-8648.

Tanzarella S, Muceli S, Santello M, Farina D (2021) Synergistic Organization of Neural Inputs from Spinal Motor Neurons to Extrinsic and Intrinsic Hand Muscles. J Neurosci 41:6878-6891.

ter Haar Romeny BM, van der Gon JJ, Gielen CC (1984) Relation between location of a motor unit in the human biceps brachii and its critical firing levels for different tasks. Experimental neurology 85:631-650.

Thompson CK, Negro F, Johnson MD, Holmes MR, McPherson LM, Powers RK, Farina D, Heckman CJ (2018) Robust and accurate decoding of motoneuron behaviour and prediction of the resulting force output. J Physiol 596:2643-2659.

Ting LH, Chiel HJ, Trumbower RD, Allen JL, McKay JL, Hackney ME, Kesar TM (2015) Neuromechanical principles underlying movement modularity and their implications for rehabilitation. Neuron 86:38-54.

Tresch MC, Jarc A (2009) The case for and against muscle synergies. Curr Opin Neurobiol 19:601-607.

Tresch MC, Saltiel P, Bizzi E (1999) The construction of movement by the spinal cord. Nat Neurosci 2:162-167.

Trypidakis G, Amiridis IG, Enoka R, Tsatsaki I, Kellis E, Negro F (2021) Ankle Angle but Not Knee Angle Influences Force Fluctuations During Plantar Flexion. Int J Sports Med.

Vecchio AD, Farina D (2019) Interfacing the neural output of the spinal cord: robust and reliable longitudinal identification of motor neurons in humans. J Neural Eng 17:016003.

Yaron A, Kowalski D, Yaguchi H, Takei T, Seki K (2020) Forelimb force direction and magnitude independently controlled by spinal modules in the macaque. Proc Natl Acad Sci U S A 117:27655-27666.